Physica Medica 59 (2019) 100–106

Contents lists available at ScienceDirect

Physica Medica

journal homepage: www.elsevier.com/locate/ejmp

Original paper

Impact of inline magnetic fields on dose distributions for VMAT in lung tumor

Takahiro Kubota[a], Fujio Araki[b,*], Takeshi Ohno[b]

[a] Graduate School of Health Sciences, Kumamoto University, 4-24-1 Kuhonji, Kumamoto, Japan
[b] Department of Health Sciences, Faculty of Life Sciences, Kumamoto University, 4-24-1 Kuhonji, Kumamoto, Japan

ARTICLE INFO

Keywords:
MRI-guided radiation therapy
Lung tumor
Dose distribution
Monte Carlo method

ABSTRACT

The purpose of this study is to investigate the impact of inline magnetic field on dose distribution for volumetric modulated arc therapy (VMAT) in lung tumors located at the chest wall and mediastinum. Two VMAT plans for a thorax phantom with lung tumors of 1 cm and 2 cm in diameter located at the chest wall were created by a treatment planning system. Next, five clinical VMAT plans for a non-small cell lung cancer (NSCLC) at early stages I and II of 5 cm or less in diameter were also used. The planning target volume (PTV) sizes were in the range from 11.1 to 82.7 cm^3. The prescription dose was 60 Gy for D_{95} in the PTV. The VMAT dose distributions without and with uniform inline magnetic field of 0.5 T and 1.0 T were calculated using the Monte Carlo method. The dose distributions were analyzed by dose volume histograms, dose differences, and dose indices. In all VMAT plans, the PTV dose was enhanced by inline magnetic field. The dose enhancement was larger with 1.0 T than with 0.5 T. In phantom plans, D_{98} in the PTV with 0.5 T and 1.0 T increased by 2.9–6.6 Gy and 3.9–9.8 Gy, respectively, in comparison with that at 0 T. Similarly, in clinical plans, it increased by 2.2–6.0 Gy and 3.9–10.7 Gy, respectively. Thus, the VMAT with the inline magnetic field was proved useful for the dose enhancement in the lung tumor located at the chest wall and mediastinum.

1. Introduction

Recently, magnetic resonance image-guided radiation therapy (MRIgRT), which combines a linear accelerator (linac) and magnetic resonance (MR) scanner, has been developed in some institutions [1–8]. The MRIgRT system is classified into two types according to a magnetic field direction. One has the transverse magnetic field vertical to an irradiation beam (head-foot direction), and the other has the inline magnetic field parallel to the irradiation beam. ViewRay [1–3] has developed an MRIgRT system equipped with three-headed ^{60}Co sources and a 6 MV linac with a low transverse field MR scanner of 0.35 T. Elekta [4,5] has developed an MRIgRT system equipped with a 6 MV linac with a high transverse field MR scanner of 1.5 T. Alberta Health Services [6] has developed an MRIgRT system equipped with a 6 or 10 MV linac with an inline magnetic field MR scanner of 0.5 T. Australian MRI-Linac program [7] has developed an MRIgRT system equipped with a 4 or 6 MV linac with an inline magnetic field MR scanner of 1.0 T. The main advantage of the MRIgRT is that it can acquire images with excellent soft tissue contrast in comparison with conventional cone-beam computed tomography (CBCT). It also has the potential to detect organ motion during irradiation, owing to the real-time imaging. In addition, it can take an image in the arbitrary cross-section of interest. In particular, the MRIgRT is expected to improve the outcome of treating lung cancers with large movement of a few centimeters [8,9].

Moreover, secondary electrons produced by the incident photon beam in media are deflected by the Lorentz force generated by the transverse magnetic field. Thus, the dose distribution produced by the electrons becomes distorted [10–15]. Furthermore, the effect of dose distribution under the magnetic field affects the lungs more, because the secondary electrons range is longer in low density media. Raaijmakers et al. [14] reported that the dose increment caused by the electron return effect (ERE) under transverse magnetic fields occurs at the tissue–lung interface. The ERE distorts dose distribution and makes skin dose to increase.

On the other hand, the effect of the inline magnetic field on the dose distribution is quite different from that of the transverse magnetic field. Several studies of a magnetic field application parallel to the irradiation beam have been conducted not assuming MRIgRT [16–21]. These studies reported that the application of a magnetic field parallel to the irradiation beam resulted in an increase of the dose. There are also two studies of radiation therapy of the lung cancer under the inline magnetic field assuming MRIgRT. Kirkby et al. [22] indicated that the

* Corresponding author.
E-mail address: f_araki@kumamoto-u.ac.jp (F. Araki).

https://doi.org/10.1016/j.ejmp.2019.03.003
Received 1 September 2018; Received in revised form 1 March 2019; Accepted 5 March 2019
Available online 09 March 2019

planning target volume (PTV) dose in the inline magnetic field was enhanced by secondary electrons deflected by the Lorentz force using non-clinical plans for three-dimensional conformal radiation therapy (3D-CRT) with 5-fields in lung tumor. Oborn et al. [23] demonstrated that the dose increment in the PTV caused by the inline magnetic field depended on the location, size, and density in the PTV using a generic cylindrical phantom and six clinical plans for 3D-CRT or intensity modulated radiation therapy (IMRT) in lung tumor. The lung dose increased when the irradiation field was small and the number of irradiation beams increased. The local dose increased more than 30% for 8 irradiation fields of 1×1 cm. Particularly, the dose in the PTVs of $\leq 15\ cm^3$ or in an isolated lung tumor increased more. However, the local dose for 8 irradiation fields of 5×5 cm was an increase up to only 5%, that is, the dose in the PTVs of $> 15\ cm^3$ or in lung tumors located at the chest wall and mediastinum did not increase significantly. Thus, the inline magnetic field MRIgRT for 3D-CRT and IMRT is expected to improve the outcome of treating small lung cancers by increasing the PTV dose.

Meanwhile, volumetric modulated arc therapy (VMAT) is used widely in the peripheral lung tumor [24–27]. The VMAT consists of the large numbers of irradiation beams with small fields. Hence, VMAT is expected to provide a better optimized dose distribution than 3D-CRT and IMRT for lung tumors located at the chest wall and mediastinum. The objective of this study is to investigate the impact of the inline magnetic field on the dose distribution for VMAT in lung tumors located at the chest wall and mediastinum, using two phantom plans and five clinical plans. The VMAT dose distributions were analyzed by dose volume histograms (DVHs) and dose indices for the conditions without and with inline magnetic flux densities of 0.5 T and 1.0 T.

2. Materials and methods

2.1. VMAT treatment planning in lung tumor

2.1.1. Thorax phantom

A thorax phantom with a lung tumor (Dynamic Thorax Phantom Model 008A, CIRS, USA) was used to calculate VMAT dose distributions in the inline magnetic flux densities of 0 T, 0.5 T, and 1.0 T. The tumor diameters were 1 cm and 2 cm for Phantoms 1 and 2, respectively. The densities of lung and tumor were approximately $0.17\ g/cm^3$ and $1.00\ g/cm^3$, respectively. The lung density was lower than $0.26\ g/cm^3$ defined by the International Commission on Radiation Units and Measurements (ICRU) Report 46 [28]. The lung tumor was located at the chest wall. The CT images were acquired with a slice thickness of 2.5 mm by using a multidetector computed tomography (MDCT) scanner (Lightspeed RT 16, GE Healthcare, Chicago, IL, USA). The acquired CT images were transferred to an Eclipse treatment planning system (TPS, ver. 10.028) (Varian Medical Systems, Palo Alto, CA, USA), and the target volumes were contoured. For the PTV, 0.5 cm and 1.0 cm margins were added to the exteriors of gross tumor volumes (GTV) with diameters of 1 cm and 2 cm, respectively. The PTVs were defined by diameters of 2 cm and 4 cm and volumes of $3.1\ cm^3$ and $43.9\ cm^3$, respectively. The organs at risk (OARs) were set to the bilateral lungs and spinal cord.

2.1.2. Clinical lung tumors

The VMAT treatment plans were created by the Eclipse TPS for five patients with non-small cell lung cancer (NSCLC) at early stages I and II with 5 cm or less in the tumor diameter. The characteristics of VMAT treatment plans for five patients are summarized in Table 1. The VMAT plans were prepared for the lung tumors located at the chest wall and mediastinum depending on the tumor size and its location. For the positioning, the chest wall was immobilized to manage the respiratory motion of less than 5 mm. Three-dimensional (3D) and four-dimensional (4D) CT images were acquired with a 2.5-mm-thick slice by using a MDCT scanner. The 3D and 4D CT images were transferred to the Eclipse TPS. The target volumes and OARs were contoured by medical physicists and radiation oncologists. The GTV was delineated from the 3D CT images. The internal target volume (ITV) was delineated from the maximum intensity projection (MIP) which was reconstructed using the 4D CT images. The PTV was defined as ITV plus 3–7 mm around it, which was determined by taking into account the PTV dose associated with the setup reproducibility and respiration motion in the patient. The PTV sizes were in the range from 11.1 to $82.7\ cm^3$. In addition, the bilateral lungs, trachea, esophagus, and spinal cord were also set as OARs.

Table 1
Characteristics of VMAT treatment plans for 2 phantoms and 5 patients.

	PTV [cm^3]	Tumor location	Number of arcs	Gantry start angle – end angle	
Phantom 1	3.1	LU	1	0–179	
Phantom 2	43.9	LU	1	0–179	
Patient 1	50.6	LU	2	179–315	215–181
Patient 2	15.5	LU	2	0–179	179–0
Patient 3	82.7	LU	1	0–179	
Patient 4	11.1	RU	2	181–30	135–179
Patient 5	29.8	RU	2	181–310	105–179

LU: left upper lobe. RU: right upper lobe.

2.1.3. VMAT dose calculations without magnetic field

The dose distributions for seven VMAT plans in lung tumors were calculated using the Acuros XB (AXB) algorithm in the Eclipse TPS. Plan optimization was performed to guarantee that the prescribed dose covered D_{95} (a dose that covers 95% of the volume) in the PTV. The prescribed dose for all VMAT plans was set to 60 Gy/10 fractions. The calculation grid size was $2.5 \times 2.5 \times 2.5$ mm. The photon energy was 6 MV from a Novalis Tx linear accelerator equipped with a high-definition 120 multileaf collimator (HD120 MLC, BrainLAB, Feldkirchen, Germany and Varian Medical Systems, Palo Alto, CA, USA). The HD120 MLC consisted of 32 pairs of leaves, each 2.5 mm wide, and 28 pairs of leaves, each 5 mm wide. The dosimetric leaf gap (DLG) was set to 0.988 mm based on the commissioning measurements.

2.2. Monte Carlo VMAT dose calculations with magnetic field

The BEAMnrc user code [29,30] based on the EGSnrc system [31,32] was used to model the radiation head of a Novalis Tx linear accelerator with the HD120 MLC. The beam modeling accuracy in the Monte Carlo (MC) simulations was verified by comparing the calculation dose distributions with those measured in a water phantom. The VMAT dose distributions for the inline magnetic flux densities of 0 T, 0.5 T, and 1.0 T were calculated using source 21 in the EGSnrc/DOSXYZnrc code [33] with the electromagnetic transport macros. Source 21 constitutes the synchronized BEAM simulation source. The irradiation parameters (i.e., coordinates of the isocenter, position of the MLC and jaws, collimator and gantry angles, and monitor unit index) for the MC calculations were exported as a DICOM-RT file from the TPS and then converted to input files in the BEAMnrc and DOSXYZnrc codes by using the DICOM-RT toolbox in the MATLAB software (MathWorks, Natick, MA, USA) [33].

The tip positions of the HD120 MLC were adjusted geometrically and offset to fit the radiation field at the isocenter plane according to the offset tables for the leaf tip positions provided by Varian. The fitting of offset tables was implemented by the approximation expression. Similarly, the phantom CT images in the DICOM-RT file were converted to a voxel-based phantom with MATLAB by using the conversion curve of the CT number to materials (air, lung, soft tissue, and bone) and mass density.

In the simulation, the directional bremsstrahlung splitting (DBS) number was set to 1000 in the BEAMnrc code. The photon splitting number was set to 128 in the DOSXYZnrc code. The photon and

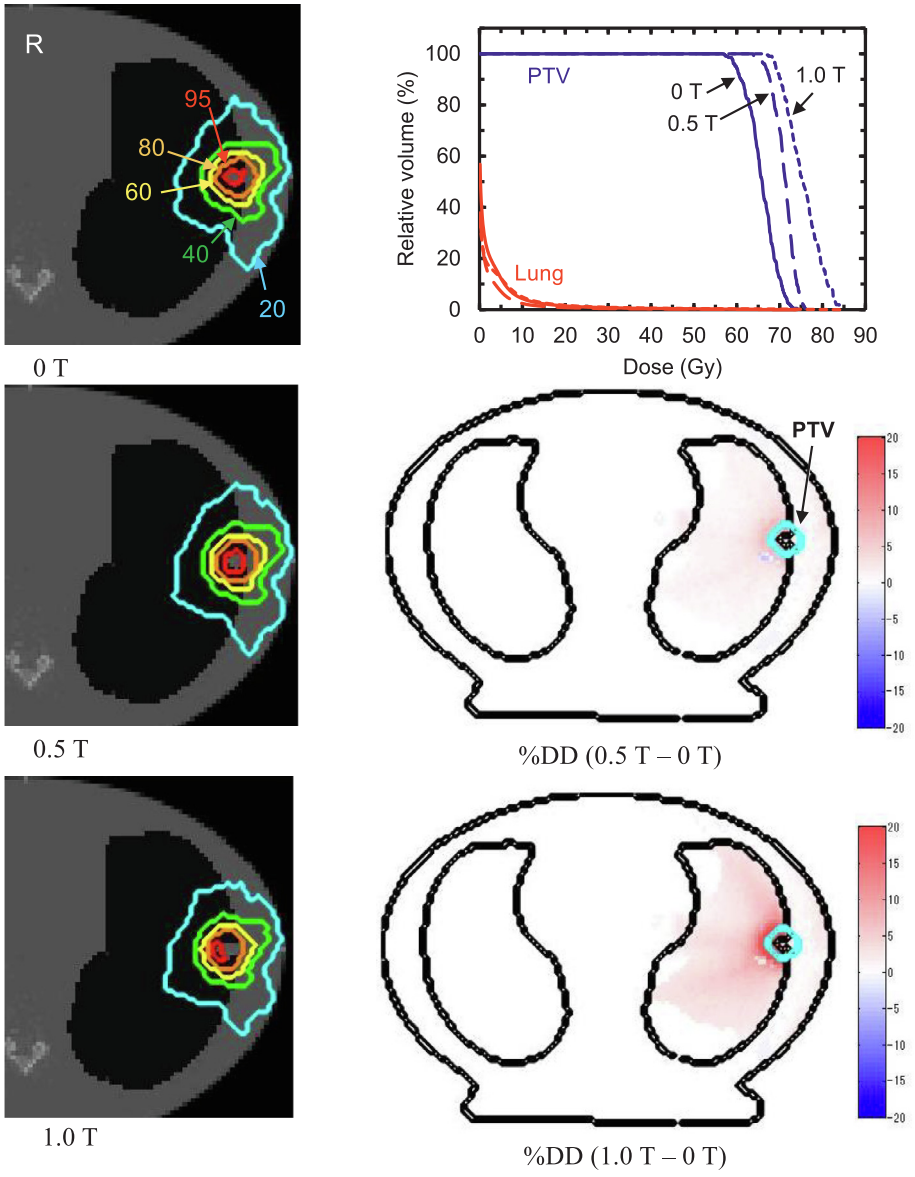

Fig. 1. Dose distributions and DVHs for 0 T, 0.5 T, and 1.0 T, and dose difference (DD) maps (%) between (0.5 T–0 T) and (1.0 T–0 T) for VMAT in Phantom 1. Dose distributions are indicated by isodose lines of 95%, 80%, 60%, 40%, and 20%.

Table 2
Dose indices in PTV and OARs for VMAT with inline magnetic field for Phantoms 1 and 2.

	Magnetic flux density [T]	PTV			Lungs		Spinal cord
		D_{98} [Gy]	D_{mean} [Gy]	HI	D_{mean} [Gy]	V_{20} [%]	D_{max} [Gy]
Phantom 1	0	59.0	65.5	0.20	2.1	1.4	6.0
	0.5	65.6	70.7	0.14	1.3	0.8	5.8
	1.0	68.8	75.2	0.19	2.0	0.9	5.9
Phantom 2	0	58.2	63.9	0.16	3.7	3.9	6.6
	0.5	61.1	66.8	0.14	3.6	4.2	6.8
	1.0	62.1	70.3	0.22	3.4	4.2	6.8

electron cutoff energies were set to 10 keV and 700 keV, respectively, and the calculation voxel size was the same (2.5 × 2.5 × 2.5 mm) as that of the AXB. The statistical uncertainty of the calculated doses was less than 1% at the isocenter point. The MC-calculated depth dose was calibrated by using the absorbed dose to water/particle per monitor unit at a central axis depth of 10 cm for a 10 × 10-cm field at a source-to-axis distance of 100 cm.

2.3. Dose evaluation

The impact of the inline magnetic field on the dose distribution was evaluated by the dose difference (DD) map and dose indices (D_{98}, D_2, and D_{mean} in PTV, V_{20} and D_{mean} in bilateral lungs, V_{40} in trachea, V_{40} in esophagus, and D_{max} in spinal cord) from DVHs. The DD was analyzed from the dose distributions calculated by the MC method with in-

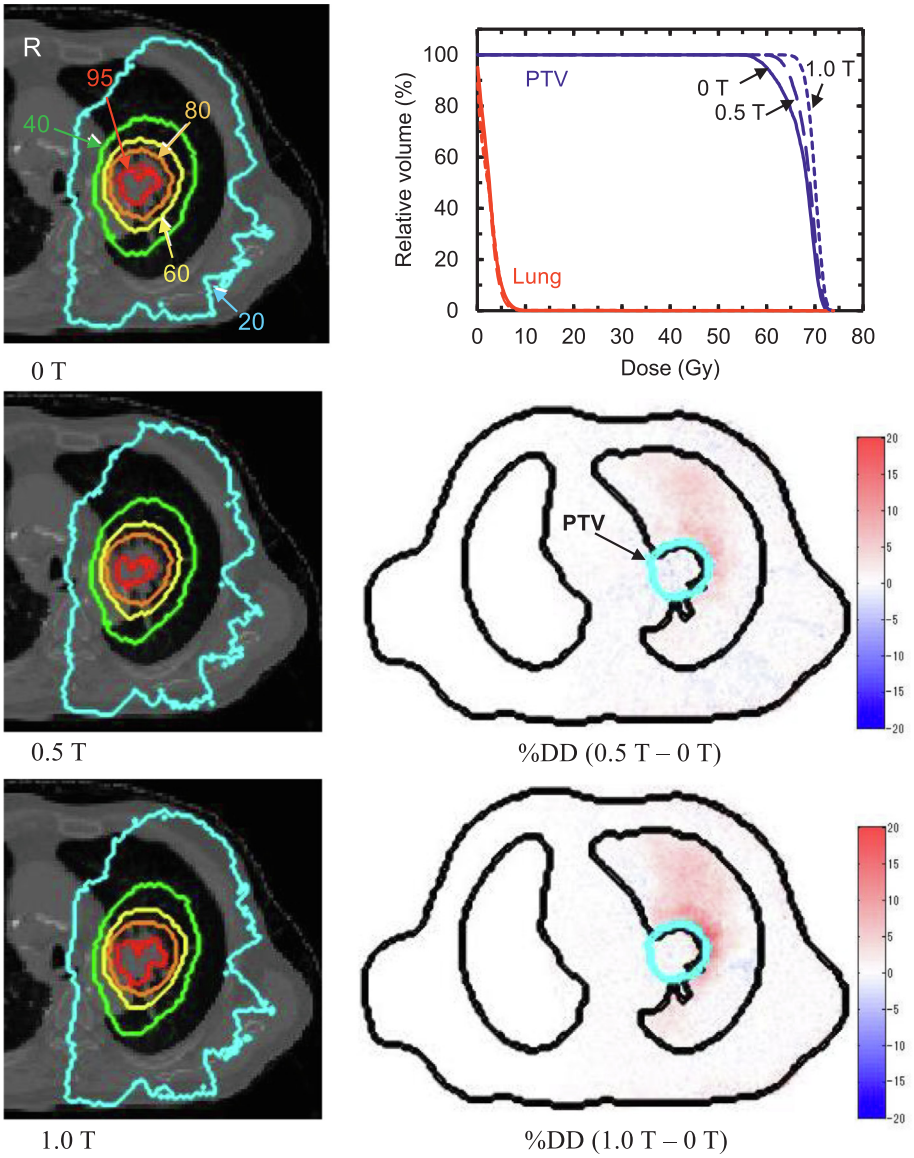

Fig. 2. Dose distributions and DVHs for 0 T, 0.5 T, and 1.0 T, and DD maps (%) between (0.5 T–0 T) and (1.0 T–0 T) for VMAT in Patient 1. Dose distributions are indicated by isodose lines of 95%, 80%, 60%, 40%, and 20%.

house software developed by MATLAB as follows:

$$\%\mathrm{DD} = \frac{D_{\mathrm{B}} - D_{\mathrm{B}=0}}{D_{\mathrm{prescribed}}} \times 100, \tag{1}$$

where D_{B} and $D_{\mathrm{B}=0}$ represent the doses at each voxel with and without the magnetic field B, respectively. $D_{\mathrm{prescribed}}$ is the prescribed dose. The dose threshold was set to 10% of the prescribed dose.

The homogeneity index (HI) was defined according to the ICRU Report 83 [34] as follows:

$$\mathrm{HI} = \frac{D_2 - D_{98}}{D_{50}} \tag{2}$$

where D_2, D_{98}, and D_{50} represent the dose covering 2%, 98%, and 50% of the PTV, respectively. HI is desired to be low.

3. Results

3.1. VMAT dose calculations for thorax phantom

Fig. 1 represent dose distributions, %DD maps, and DVHs for the inline magnetic flux densities of 0 T (no magnetic field), 0.5 T, and 1.0 T for VMAT in Phantom 1. Table 2 presents dose indices in PTV and OARs. In all cases, the doses in the PTV with non-zero magnetic field were higher compared to that of 0 T. The DD was particularly large at the peritumoral area in lung. The increment of dose in PTV was higher for 1.0 T than for 0.5 T. In Phantom 1, D_{98} in the PTV at 0.5 T and 1.0 T increased by 6.6 Gy and 9.8 Gy, respectively, compared with that at 0 T. Similarly, D_{mean} at 0.5 T and 1.0 T in the PTV increased by 5.2 Gy and 9.7 Gy, respectively. In Phantom 2, D_{98} at 0.5 T and 1.0 T in the PTV increased by 2.9 Gy and 3.9 Gy, respectively, compared with that at 0 T. Similarly, D_{mean} at 0.5 T and 1.0 T increased by 2.9 Gy and 6.4 Gy, respectively. HI had a tendency to decrease at 0.5 T and was no significant difference at 1.0 T compared with 0 T. There was no significant dose difference in OARs.

3.2. VMAT dose calculation for clinical lung tumors

Figs. 2 and 3 represent dose distributions, %DD maps, and DVHs for the inline magnetic flux densities of 0 T (no magnetic field), 0.5 T, and 1.0 T for VMAT for typical Patients 1 and 4, respectively. Tables 3 and 4

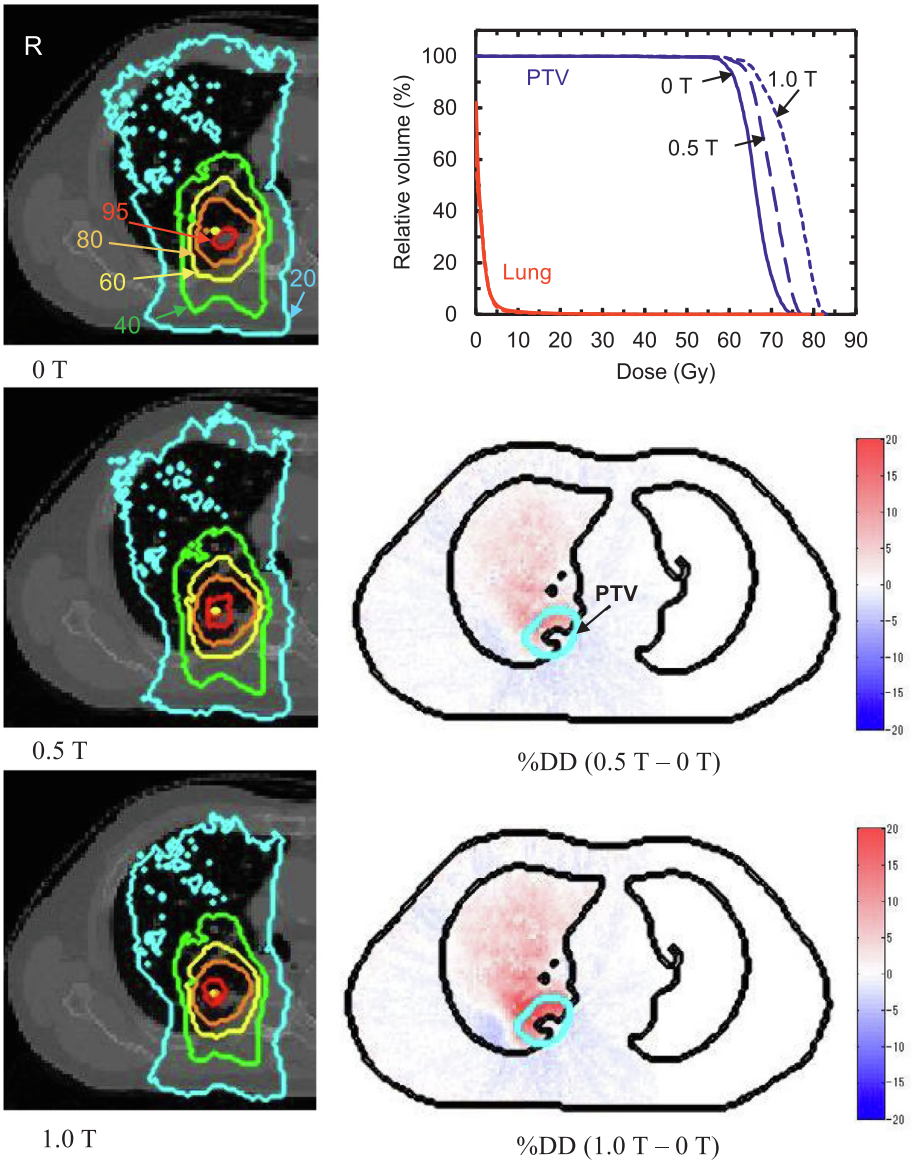

Fig. 3. Dose distributions and DVHs for 0 T, 0.5 T, and 1.0 T, and DD maps (%) between (0.5 T–0 T) and (1.0 T–0 T) for VMAT in Patient 4. Dose distributions are indicated by isodose lines of 95%, 80%, 60%, 40%, and 20%.

Table 3
Dose indices in PTV for VMAT with inline magnetic field for Patients 1–5.

	Magnetic flux density [T]	D_{98} [Gy]	D_{mean} [Gy]	HI
Patient 1	0	58.1	67.4	0.20
	0.5	62.7	68.6	0.14
	1.0	66.4	70.0	0.09
Patient 2	0	58.8	68.4	0.27
	0.5	64.8	71.6	0.18
	1.0	69.5	75.3	0.12
Patient 3	0	57.8	66.3	0.20
	0.5	60.0	67.3	0.17
	1.0	61.7	68.4	0.15
Patient 4	0	58.3	64.8	0.23
	0.5	61.1	69.9	0.22
	1.0	63.7	74.7	0.27
Patient 5	0	56.8	66.8	0.21
	0.5	61.1	68.0	0.15
	1.0	63.7	69.4	0.12

present dose indices in PTV and OARs, respectively. In all cases, the doses in the PTV with non-zero magnetic field were higher compared to that of 0 T, as well as in the cases of phantoms. The DD was larger at the lung tissue around the PTV. The dose in the PTV increased more at 1.0 T than at 0.5 T. For Patients 1–5, D_{98} in the PTV at 0.5 T and 1.0 T increased by 2.2–6.0 Gy and 3.9–10.7 Gy, respectively, compared with that at 0 T. Similarly, D_{mean} in the PTV at 0.5 T and 1.0 T increased by 1.0–5.0 Gy and 2.1–9.6 Gy, respectively. For D_{98}, the largest dose increment was for the small tumor located at the chest wall of Patient 2. The largest D_{mean} increment was for the paravertebral small lung tumor in Patient 4. HI at 0.5 and 1.0 T approached zero in almost all patients, except Patient 4 at 1.0 T. There was no significant dose difference in the OARs.

4. Discussion

In all VMAT plans, the dose in PTV was enhanced by the inline magnetic field. The effect was more remarkable when the irradiation field was small and the number of irradiation beams was increased. From the expression for the gyroradius of the secondary electrons, the

Table 4
Dose indices in OARs for VMAT with inline magnetic field for Patients 1–5.

	Magnetic flux density [T]	Lungs		Trachea	Esophagus	Spinal cord
		D_{mean} [Gy]	V_{20} [%]	V_{40} [%]	V_{40} [%]	D_{max} [Gy]
Patient 1	0	2.7	0.1	0.0	0.0	18.6
	0.5	2.6	0.1	0.0	0.0	19.1
	1.0	2.5	0.1	0.0	0.0	18.9
Patient 2	0	10.4	17.3	0.0	0.0	8.5
	0.5	13.5	20.3	0.0	0.0	8.4
	1.0	14.1	20.9	0.0	0.0	8.6
Patient 3	0	8.1	16.6	0.0	0.0	12.6
	0.5	8.4	17.0	0.0	0.0	12.4
	1.0	8.6	17.1	0.0	0.0	12.3
Patient 4	0	1.5	0.3	0.2	0.0	30.0
	0.5	1.3	0.3	0.1	0.0	28.9
	1.0	1.3	0.3	0.2	0.0	28.9
Patient 5	0	2.7	2.6	0.0	0.0	9.3
	0.5	3.2	3.3	0.0	0.0	9.5
	1.0	3.4	3.5	0.0	0.0	9.4

dose increment should be larger for 1.0 T than for 0.5 T. In the inline magnetic field, when a secondary electron enters the magnetic field at a certain angle, it continues traveling while drawing a spiral trajectory along the beam axis. In this case, the gyroradius of the secondary electrons becomes smaller than the gyroradius of the secondary electrons in the transverse magnetic field. The gyroradius r is expressed as follows:

$$r = \frac{m v \sin\theta}{eB} \quad (0 \leqslant \sin\theta \leqslant 1) \tag{3}$$

where m is the electron mass (kg), v is the electron velocity (m/s), e is the quantum of electricity (C), B is the magnetic flux density (T), and θ is the angle of secondary electrons incident on the inline magnetic field (the angle between v and B).

The radius of the spiral trajectory of secondary electrons in the inline magnetic field depends on the incident angle θ between the secondary electrons velocity and the magnetic flux density vector B, as shown in Eq. (3). The trajectories of secondary electrons at 0 T are spread out to both sides in lung, but secondary electrons in the inline magnetic field are focused toward the central beam axis along the inline magnetic field. At the same time, the larger the magnetic flux density is, the smaller the gyroradius of the secondary electrons becomes. The spread of secondary electrons to both sides is suppressed by the inline magnetic field; therefore, the dose along the beam central axis is enhanced. As a result, the irradiation field decreases, and, thus, the penumbra reduces. In this study, the mean electron energy was 1.13 MeV, which was obtained from the electron fluence spectrum of a 5 × 5-cm field using the EGSnrc/flurznrc code [35]. For $\theta = 90$, the gyroradiuses at 0.5 T and 1.0 T were 1.0 cm and 0.5 cm, respectively. Thus, the focusing effect of secondary electrons is stronger at 1.0 T than at 0.5 T.

In this study, the PTV dose increment in Phantom 2 was smaller than that of Phantom 1 as shown in Table 2. D_{98} for the PTV of 3.1 cm^3 and 43.9 cm^3 at 1.0 T increased by 9.8 Gy (16.6%) and 3.9 Gy (6.7%), respectively, in compared with that at 0 T. Oborn et al. [23] have reported that the dose increment was approximately 20% and 5% for the PTV of 3 cm^3 and 40 cm^3, respectively, for IMRT and 3D-CRT at 1.0 T. The result was similar to that of Oborn et al. [23]. The dose enhancement is associated with the irradiation technique, the tumor location, and the margin size.

In all clinical VMAT plans, the PTV dose increased when the irradiation field was small and the number of irradiation beams increased. The largest enhancement of D_{98} was observed in Patient 2. It can be attributed to the small PTV size. Meanwhile, D_{mean} and V_{20} in lungs at 1.0 T increased by 2.8 Gy and 3.6%, respectively, in compared with those at 0 T. Moreover, the largest D_{mean} enhancement was observed in Patient 4. It, in turn, can be attributed to the small PTV size and large number of beams irradiated to the PTV through the lung region. According to Oborn et al. [21], the PTV dose increment was not significant in three of six cases for 3D-CRT and IMRT: two cases of the lung tumor (PTV: 28, 55 cm^3) located at the mediastinum and one case of tumor (PTV: 31 cm^3) located at the chest wall. These cases were similar to Patient 1 and Patient 5. The PTV located at the mediastinum in Patient 1 was of large size, but the PTV dose was increased. The number of irradiation beams passed through the lung was increased compared to 3D-CRT and IMRT, and, consequently, the dose of the beam central axis was enhanced. There was a similar tendency in Patient 5 with the lung tumor located at the chest wall.

From results in this study, the VMAT dose distributions in the inline magnetic fields are expected to increase the dose to the lung tumor. In particular, the VMAT is more effective on the PTV dose enhancement than for 3D-CRT and IMRT, especially for eccentric lung tumors located at the chest wall and mediastinum. This is because the secondary electrons in a low-density area surrounding the tumor are focused toward the central beam axis in proportion to the number of irradiation beams. This is more effective for a small field in a low-density area.

Meanwhile, the inline magnetic field-MRIgRT can reduce the ITV margin delineated without the magnetic field. However, the inline magnetic field also reduces the field penumbra [36]. Sarah et al. [36] quantified the small reduction of the penumbra by the inline magnetic fields of 0.9 T and 1.5 T; reduction of 0.1–2.5 mm for 0.9 T and 0.1–4.4 mm for 1.5 T depending on the lung depth from the chest wall. Therefore, the PTV margin is necessary to cover the PTV dose considering the reduction of penumbra. The ITV margin is deeply associated with the PTV dose enhancement. Finally, the ITV and PTV margins may be no longer necessary for the targets with on-line MRI guided treatments. In this case, the PTV dose enhancement also reduces as the margins with a low-density area decrease.

In addition, the dose to OARs was no significant difference. This means it is possible to decrease the OAR dose by reducing the monitor unit (MU) owing to the PTV dose increment in the inline magnetic field, compared to the MU without the magnetic field in the treatment planning. In this study, the skin dose increment due to the inline magnetic field could not be considered. The skin dose increment due to a convergence of the electron contamination by the inline magnetic field remains a concern [6,37–39]. However, it is expected that the skin dose enhancement is small because the irradiation field in VMAT is

relatively small.

5. Conclusions

The impact of inline magnetic field on dose distribution was investigated for VMAT in the lung tumors located at the chest wall and mediastinum. In all VMAT cases, the PTV dose in inline magnetic field increased compared to zero-magnetic-field case. The dose enhancement was larger at 1.0 T than at 0.5 T; also, it was larger for small lung tumors. D_{98} and D_{mean} in the PTV increased by up to 10.7 Gy and 9.6 Gy at 1.0 T, respectively. In contrast, the dose to lungs and other OARs was without an increase. The dose enhancement in PTV depended on the margin size as well as the PTV size and also tumor locations. Consequently, the VMAT in the inline magnetic field was found useful for the dose enhancement in the lung tumor located at the chest wall and mediastinum.

Acknowledgements

The authors would like to thank the staff at the Kumamoto Radiosurgery Clinic for providing the clinical VMAT plans.

References

[1] Mutic S, Dempsey JF. The ViewRay system: magnetic resonance-guided and controlled radiotherapy. Semin Radiat Oncol 2014;24:196–9. https://doi.org/10.1016/j.semradonc.2014.02.008.
[2] Mutic S, Low D, Chmielewski T, Fought G, Gerganov G, Hernandez M, et al. The design and implementation of a novel compact linear accelerator-based magnetic resonance imaging-guided radiation therapy (MR-IGRT) system. Int J Radiat Oncol Biol Phys 2016;96:E641. https://doi.org/10.1016/j.ijrobp.2016.06.2234.
[3] Liney GP, Whelan B, Oborn B, Barton M, Keall P. MRI-linear accelerator radiotherapy systems. Clin Oncol 2018;30:686–91. https://doi.org/10.1016/j.clon.2018.08.003.
[4] Lagendijk JJW, Raaymakers BW, van Vulpen M. The magnetic resonance imaging-linac system. Semin Radiat Oncol 2014;24:207–9. https://doi.org/10.1016/j.semradonc.2014.02. 009.
[5] Raaymakers BW, Lagendijk JJW, Overweg J, Kok JGM, Raaijmakers AJE, Kerkhof EM, et al. Integrating a 1.5 T MRI scanner with a 6 MV accelerator: proof of concept. Phys Med Biol 2009;54:N229–37. https://doi.org/10.1088/0031-9155/54/12/N01.
[6] Keyvanloo A, Burke B, St Aubin J, Baillie D, Wachowicz K, Warkentin B, et al. Minimal skin dose increase in longitudinal rotating biplanar linac-MR systems: examination of radiation energy and flattening filter design. Phys Med Biol 2016;61:3527–39. https://doi.org/10.1088/0031-9155/61/9/3527.
[7] Keall PJ, Barton M, Crozier S. The Australian magnetic resonance imaging-linac program. Semin Radiat Oncol 2014;24:203–6. https://doi.org/10.1016/j.semradonc.2014.02.015.
[8] Menten MJ, Wetscherek A, Fast MF. MRI-guided lung SBRT: present and future developments. Phys Medica 2017;44:139–49. https://doi.org/10.1016/j.ejmp.2017.02.003.
[9] Keall PJ, Mageras GS, Balter JM, Emery RS, Forster KM, Jiang SB, et al. The management of respiratory motion in radiation oncology report of AAPM Task Group 76. Med Phys 2006;33:3874–900. https://doi.org/10.1118/1.2349696.
[10] Raaymakers BW, Raaijmakers AJE, Kotte ANTJ, Jette D, Lagendijk JJW. Integrating a MRI scanner with a 6 MV radiotherapy accelerator: dose deposition in a transverse magnetic field. Phys Med Biol 2004;49:4109–18. https://doi.org/10.1088/0031-9155/49/17/019.
[11] Yang YM, Bednarz B. Consistency evaluation between EGSnrc and Geant4 charged particle transport in an equilibrium magnetic field. Phys Med Biol 2013;58.. https://doi.org/10.1088/0031-9155/58/4/N47.
[12] Raaijmakers AJE, Raaymakers BW, Lagendijk JJW. Integrating a MRI scanner with a 6 MV radiotherapy accelerator: dose increase at tissue-air interfaces in a lateral magnetic field due to returning electrons. Phys Med Biol 2005;50:1363–76. https://doi.org/10.1088/0031-9155/50/7/002.
[13] Erkelens CJ, Raaijmakers AJE, Lagendijk JJW. Integrating a MRI scanner with a 6 MV radiotherapy accelerator: impact of the surface orientation on the dose deposition at interfaces. Phys Med Biol 2007;52:929–39. https://doi.org/10.1088/0031-9155/52/4/005.
[14] Raaijmakers AJE, Raaymakers BW, Lagendijk JJW. Magnetic-field-induced dose effects in MR-guided radiotherapy systems: dependence on the magnetic field strength. Phys Med Biol 2008;53:909–23. https://doi.org/10.1088/0031-9155/53/4/006.
[15] Kirkby C, Stanescu T, Rathee S, Carlone M, Murray B, Fallone BG. Patient dosimetry for hybrid MRI-radiotherapy systems. Med Phys 2008;35:1019–27. https://doi.org/10.1118/1.2839104.
[16] Bielajew A. The effect of strong longitudinal magnetic fields on dose deposition from electron and photon beams. Med Phys 1993;20:1171–9.
[17] Allen Li X, Reiffel L, Chu J, Naqvi S. Conformal photon-beam therapy with transverse magnetic fields: a Monte Carlo study. Med Phys 2001;28:127–33. https://doi.org/10.1118/1.1344207.
[18] Pillsbury R. Control of photon beam dose profiles by localized transverse magnetic fields. Phys Med Biol 2000;45:177–82.
[19] Wadi-Ramahi SJ, Naqvi SA, Chu JCH. Evaluating the effectiveness of a longitudinal magnetic field in reducing underdosing of the regions around upper respiratory cavities irradiated with photon beams – a Monte Carlo study. Med Phys 2001;28:1711–7. https://doi.org/10.1118/1.1386780.
[20] Chen Y, Bielajew AF, Litzenberg DW, Moran JM, Becchetti FD. Magnetic confinement of electron and photon radiotherapy dose: a Monte Carlo simulation with a nonuniform longitudinal magnetic field. Med Phys 2005;32:3810–8. https://doi.org/10.1118/1.2011091.
[21] Jette D. Magnetic fields with photon beams: dose calculation using electron multiple-scattering theory. Med Phys 2000;27:1705–16. https://doi.org/10.1118/1.1286554.
[22] Kirkby C, Murray B, Rathee S, Fallone BG. Lung dosimetry in a linac-MRI radiotherapy unit with a longitudinal magnetic field. Med Phys 2010;37:4722–32. https://doi.org/10.1118/1.3475942.
[23] Oborn BM, Ge Y, Hardcastle N, Metcalfe PE, Keall PJ. Dose enhancement in radiotherapy of small lung tumors using inline magnetic fields: a Monte Carlo based planning study. Med Phys 2016;43:368–77. https://doi.org/10.1118/1.4938580.
[24] Ong CL, Verbakel WFAR, Cuijpers JP, Slotman BJ, Lagerwaard FJ, Senan S. Stereotactic radiotherapy for peripheral lung tumors: a comparison of volumetric modulated arc therapy with 3 other delivery techniques. Radiother Oncol 2010;97:437–42. https://doi.org/10.1016/j.radonc.2010.09.027.
[25] Merrow CE, Wang IZ, Podgorsak MB. A dosimetric evaluation of VMAT for the treatment of non-small cell lung cancer. J Appl Clin Med Phys 2013;14:4110.
[26] Ding L, Lo Y-C, Kadish S, Goff D, Pieters RS, Graeber G, et al. Volume Modulated Arc Therapy (VMAT) for pulmonary Stereotactic Body Radiotherapy (SBRT) in patients with lesions in close approximation to the chest wall. Front Oncol 2013;3:1–6. https://doi.org/10.3389/fonc.2013.00012.
[27] Roy S, Badragan I, Ahmed SN, Sia M, Singh J, Bahl G. Integration of radiobiological modeling and indices in comparative plan evaluation: a study comparing VMAT and 3D-CRT in patients with NSCLC. Pract Radiat Oncol 2018:1–10. https://doi.org/10.1016/j.prro.2018.02.012.
[28] White GRDR, Wilson IJ. ICRU Report 46. International Commission on Radiation Units and Measurements, Bethesda, MD; 1992.
[29] Rogers DW, Faddegon BA, Ding GX, et al. BEAM: a Monte Carlo code to simulate radiotherapy treatment units. Med Phys 1995;22:503–24.
[30] Rogers DW, Walters BR, Kawrakow I. BEAMnrc user's manual. National Research Council of Canada Report PIRS-509(A) Rev L, 2013.
[31] Kawrakow I. Accurate condensed history Monte Carlo simulation of electron transport. I. EGSnrc, the new EGS4 version. Med Phys 2000;27:485–98.
[32] Kawrakow I, Rogers DW, Tessier F et al. The EGSnrc code system: Monte Carlo simulation of electron and photon transport. National Research Council of Canada Report PIRS-701, 2013.
[33] Walters B, Kawrakow I, Rogers DWO. DOSXYZnrc Users Manual. NRCC Rep PIRS-0794 2016:1–125. doi: 10.1118/1.4773883.
[34] ICRU International Commission on Radiation Units and Measurements Prescribing, recording, and reporting photon-beam intensity-modulated radiation therapy (IMRT). ICRU Report 83. J ICRU. 2010;10:1–106.
[35] Rogers DWO, Kawrakow I, Seuntjens JP, Walters BRB, Mainegra-Hing E. NRC user codes for EGSnrc. NRCC Rep PIRS-702 (Rev B) 2013;702:1–92.
[36] Sarah JA, Jarrad B, Trent C, Thahabar A, Laura G, Bin D, et al. Technical note: Penumbral width trimming in solid lung dose profiles for 0.9 and 1.5 T MRI-Linac prototypes. Med Phys 2018;45:479–87. https://doi.org/10.1002/mp.12680.
[37] Keyvanloo A, Burke B, Warkentin B, Tadic T, Rathee S, Kirkby C, et al. Skin dose in longitudinal and transverse linac-MRIs using Monte Carlo and realistic 3D MRI field models. Med Phys 2012;39:6509–21. https://doi.org/10.1118/1.4754657.
[38] Van Heijst TCF, Den Hartogh MD, Lagendijk JJW, Van Den Bongard HJGD, Van Asselen B. MR-guided breast radiotherapy: feasibility and magnetic-field impact on skin dose. Phys Med Biol 2013;58:5917–30. https://doi.org/10.1088/0031-9155/58/17/5917.
[39] Mahdavi SR, Esmaeeli AD, Pouladian M, Monfared AS, Sardari D, Bagheri S. Breast dosimetry in transverse and longitudinal field MRI-Linac radiotherapy systems. Med Phys 2015;42:925–36. https://doi.org/10.1118/1.4906193.